

Supplementary Materials for

Ozone Generation and Chemistry from 222 nm Germicidal Ultraviolet Light in a Fragrant Restroom

Michael F. Link^{1,*}, Rileigh L. Robertson¹, Andrew Shore¹, Behrang H. Hamadani¹, Christina E. Cecelski¹, Dustin G. Poppendieck^{1,*}

¹ National Institute of Standards and Technology, Gaithersburg, USA

*Corresponding authors emails: michael.f.link@nist.gov; dustin.poppendieck@nist.gov

This PDF file includes:

Supplementary Text
Figs. S1 to S17
Tables S1 to S8
References

Table of Contents

1. Quantification of terpenoid concentrations from PTR-MS and contributions to O ₃ loss from reactions with VOCs ($k_{\text{loss,VOC}}$), Fig. S1 through S4 and Tables S1 through S5.....	3
2. Differences in particle production dynamics from GUV222 with and without the use of a mixing fan, Fig. S5 and S6.....	13
3. Measurements of air change rates (ACR), Fig. S7.....	15
4. O ₃ $k_{\text{loss,VOC}}$ speciated by terpenoid, Fig. S8.....	16
5. Comparison of O ₃ production measured in the restroom compared to previous chamber study, Fig. S9.....	17
6. O ₃ Modeling, Fig. S10 through S12 and Table S6.....	18
7. Example ocimene O ₃ oxidation mechanism producing select VOC _{O₃ Ox.} byproducts, Fig. S13.....	22
8. Deposition efficiency of respired particles in three zones of the respiratory tract as a function of particle diameter, Fig. S14.....	23
9. Estimation of VOC _{cond,g} wall loss rate constant ($k_{\text{cond,w}}$) and expected ranges for $f_{\text{cond,p}}$ Fig. S15 and S16 and Table S7.....	24
10. Prediction of M _p production from speciated terpenoid reactions and secondary organic aerosol yields, Fig. S17 and Table S8.....	27

1. Quantification of terpenoid concentrations from PTR-MS and contributions to O₃ loss from reactions with VOCs ($k_{\text{loss,VOC}}$).

Operating parameters of the PTR-MS are shown in Table S1.

Table S1. PTR-MS instrument operating parameters.

PTR-MS Operating Parameters	
Focusing ion molecular reactor (fIMR) Pressure	2 mbar (200 Pa)
fIMR Temperature	60 °C
fIMR Voltage	450 V
Extraction Frequency	14 kHz
Big segmented quadrupole (BSQ) Voltage	300 V
fIMR Front and Back Voltage	600V (front), 20V (back), $\Delta V = 580V$
BSQ front voltage – Skimmer voltage	$\Delta V = 4V$
Reduced electric field strength (E/N)	134 Td ($134 \times 10^{-21} \text{ V m}^{-2}$)

Using both real-time and GC PTR-MS we measured a range of GUV222 VOC_{O₃ Ox.} byproducts (Table S2) and a suite of reactive terpenoid precursors.

Table S2. Ions measured by the PTR-MS that increased in signal when GUV222 was on. Quantifiable signals are included in the VOC_{O₃ Ox.} byproducts concentrations and generation rates reported in the main text. Categories are ALD = aldehyde, TerpOx = terpene oxidation product, and Other = other oxidized VOC. GR shown here are GR_{GUV222} as defined in the main text. Average and standard deviation are determined for five GUV222 on/off cycles. We report GR in parts-per-trillion (ppt) per hour here.

Quantified ion signals				
PTR-MS ion	Ion identity	Category	Wk1 GR (ppt h ⁻¹)	Wk2 GR (ppt h ⁻¹)
C ₃ H ₇ O ⁺	Acetone	Other	4120 ± 620	1370 ± 660
C ₂ H ₅ O ₂ ⁺	Acetic acid/ Glycolaldehyde	Other	1070 ± 740	1530 ± 800
C ₃ H ₇ O ₂ ⁺	Hydroxyacetone/propanoic acid	Other	800 ± 140	200 ± 60
C ₇ H ₁₁ O ⁺	Terpene oxidation product	TerpOx	655 ± 110	100 ± 100
C ₂ H ₅ O ⁺	Acetaldehyde	ALD	550 ± 300	710 ± 550
C ₅ H ₉ O ₂ ⁺	Terpene oxidation product	TerpOx	160 ± 60	85 ± 68
C ₄ H ₇ O ₂ ⁺	2-butenal	ALD	75 ± 52	34 ± 35
C ₄ H ₁₁ O ₂ ⁺	Butanediol	Other	83 ± 10	130 ± 30
C ₇ H ₁₁ O ₂ ⁺	Terpene oxidation product	TerpOx	45 ± 13	9 ± 5
C ₈ H ₉ O ⁺	Terpene oxidation product	TerpOx	56 ± 16	62 ± 29
C ₇ H ₇ O ⁺	Terpene oxidation product	TerpOx	55 ± 7	79 ± 39
C ₉ H ₁₉ O ⁺	Nonanal	ALD	51 ± 8	69 ± 54
C ₆ H ₁₃ O ⁺	Terpene oxidation products including hexanal/hexanone	ALD	40 ± 23	130 ± 40
C ₃ H ₆ NO ⁺	acrylamide	Other	24 ± 14	26 ± 25
C ₃ H ₇ O ₃ ⁺	Lactic acid	Other	32 ± 7	20 ± 9
C ₇ H ₁₃ O ⁺	Terpene oxidation products including heptenal	ALD	25 ± 4	13 ± 9
C ₆ H ₁₁ O ₂ ⁺	Terpene oxidation product	TerpOx	19 ± 11	14 ± 4
C ₇ H ₉ O ⁺	Terpene oxidation product	TerpOx	17 ± 7	7 ± 3
C ₇ H ₁₅ O ⁺	heptanal	ALD	23 ± 10	37 ± 18
C ₅ H ₉ O ⁺	Terpene oxidation products including pentenal	ALD	25 ± 17	22 ± 19
C ₅ H ₁₁ O ⁺	pentanal	ALD	18 ± 5	26 ± 9
C ₇ H ₁₂ NO ⁺	Terpene oxidation product	TerpOx	11 ± 2	3 ± 2
C ₁₀ H ₁₇ O ₂ ⁺	Terpene oxidation product	TerpOx	9 ± 4	3 ± 3
C ₁₀ H ₁₅ O ⁺	Terpene oxidation product	TerpOx	5 ± 4	3 ± 2
C ₁₂ H ₂₅ O ⁺	dodecanal	ALD	5 ± 1	7 ± 4
C ₁₀ H ₁₅ O ₂ ⁺	Terpene oxidation product	TerpOx	4 ± 2	2 ± 1
C ₁₀ H ₁₃ O ⁺	Terpene oxidation product	TerpOx	3 ± 1	2 ± 1
C ₉ H ₁₇ O ⁺	Terpene oxidation product	TerpOx	6 ± 5	3 ± 2
C ₁₁ H ₂₃ O ⁺	undecanal	ALD	2 ± 1	4 ± 2
C ₁₄ H ₂₉ O ⁺	tetradecanal	ALD	1 ± 1	1 ± 1
C ₉ H ₁₅ O ₂ ⁺	Terpene oxidation product	TerpOx	1 ± 1	2 ± 1
C ₁₂ H ₂₃ O ⁺	dodecenal	ALD	1 ± 1	1 ± 1
HCHO ⁺	Formaldehyde	ALD	930 ± 420	850 ± 410
HCOOH ⁺	Formic acid	Other	120 ± 70	220 ± 340
Total GR_{VOC O₃ Ox., GUV222}			9040 ± 2690	5750 ± 3330
**Unquantified ions that increased when GUV222 was on				
PTR-MS ion	Suspected Ion identity			
C ₂ H ₅ O ₃ ⁺	Terpene fragment			

$C_6H_9O^+$	Terpene fragment
$C_6H_9O_2^+$	
$C_7H_5O^+$	
$C_9H_{21}O_2^+$	Nonanal water cluster
$C_7H_{11}O_3^+$	
$C_7H_{13}O_3^+$	$C_7H_{11}O_2^+$ water cluster
$C_9H_{15}O_4^+$	Water cluster
$C_{10}H_{17}O_3^+$	$C_{10}H_{15}O_2^+$ water cluster
$C_9H_{15}O_3^+$	Water cluster
$C_{12}H_{27}O_2^+$	Dodecanal water cluster
$C_5H_7O^+$	
$C_3H_9O_2^+$	Acetone water cluster

*formaldehyde (HCHO) and formic acid (HCOOH) were measured using infrared spectroscopy.

**Cells that are blank are unidentified ions.

From online gas-chromatography measurements of reactive VOC precursors in the restroom during the weekend measurements (using GC-PTR-MS), offline static headspace analyses of a fresh urinal pad (Fig. S1), and real-time PTR-MS measurements, we identify six terpenoids that are important precursors for O₃ reactions; α -terpinene, terpinolene, linalool, limonene, and linalyl acetate.

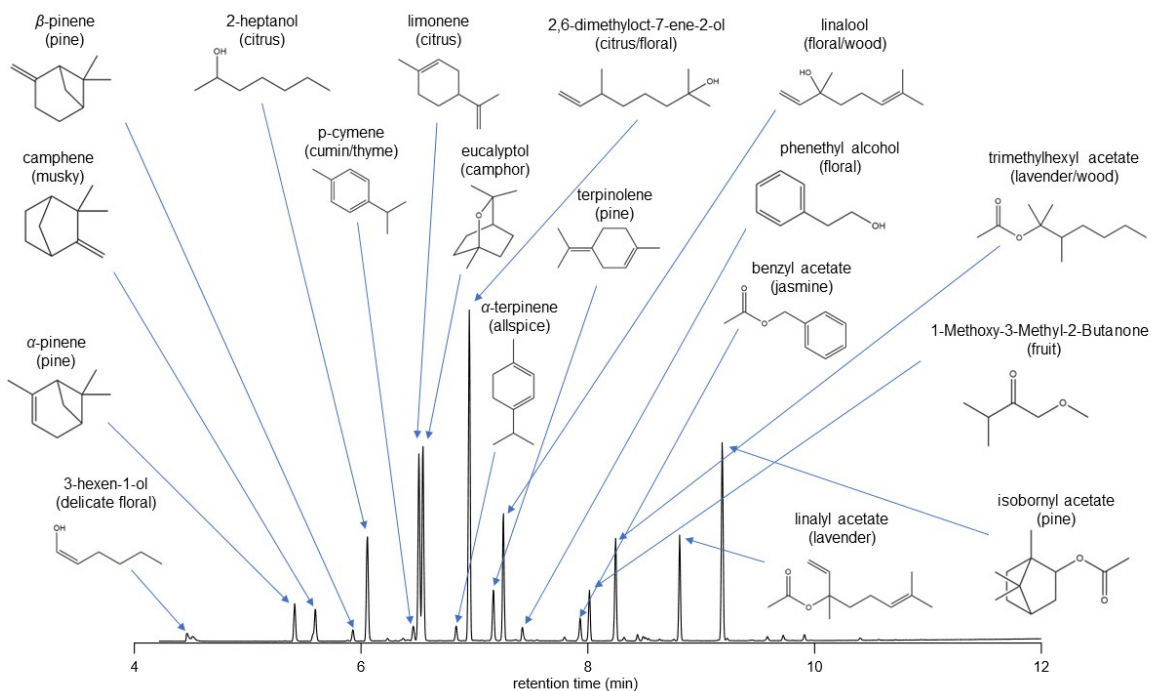


Fig. S1. GC-MS headspace chromatogram of ≈ 1 g of freshly opened urinal pad in 20 mL glass vial showing the variety of VOCs emitted from the urinal pad.

The offline static headspace urinal pad measurement helped us understand what VOCs we should look for in the PTR-MS GC measurements. We used authentic monoterpene standards made in-house (Table S3) to calibrate for most of the monoterpenes we measured in the restroom (Table S4) and quantified them from PTR-MS GC restroom measurements.

Table S3. PTR-MS calibration cylinder information.

Calibration Cylinder #1 (APE1135914)	
Calibrant	Concentration (ppb)
α -pinene	228.39
Δ 3-carene	194.47
Limonene	255.26
1,8-cineole	202.11
Calibration Cylinder #2 (APE1145325)	
β -pinene	209.0
α -terpinene	226.2
Camphene	229.7
p-cymene	171.0

Table S4. Sensitivities of terpenoids measured with PTR-MS using gas-chromatography (GC) or real-time sampling (RT). fH^+ is the fraction of the proton-transfer VOC H^+ adduct to the sum of product ions from the VOC + H_3O^+ ionization reaction used in PTR-MS.

Monoterpenes						
Terpenoid	Molecular Formula	Quant Ion	Retention Time (s)	GC Sensitivity (cnts ppb⁻¹)	RT Sensitivity (cps ppb⁻¹)	fH^+
α -pinene	C ₁₀ H ₁₆	C ₁₀ H ₁₇ ⁺	371	5.5 x 10 ⁵	3900	0.55
Limonene	C ₁₀ H ₁₆	C ₁₀ H ₁₇ ⁺	432	1.4 x 10 ⁶	1600	0.45
Camphene	C ₁₀ H ₁₆	C ₁₀ H ₁₇ ⁺	386	1.7 x 10 ⁶	4600	0.55
β -pinene	C ₁₀ H ₁₆	C ₁₀ H ₁₇ ⁺	405	1.2 x 10 ⁶	3200	0.49
α -terpinene	C ₁₀ H ₁₆	C ₁₀ H ₁₇ ⁺	426	7.2 x 10 ⁵	2000	0.54
Ocimene	C ₁₀ H ₁₆	C ₁₀ H ₁₇ ⁺	437	a	b	0.62
Terpinolene	C ₁₀ H ₁₆	C ₁₀ H ₁₇ ⁺	464	a	b	0.64
C10 Terpene Alcohols						
1,8-cineole	C ₁₀ H ₁₈ O	C ₁₀ H ₁₇ ⁺	442	1.9 x 10 ⁶	5500	
Linalool	C ₁₀ H ₁₈ O	C ₁₀ H ₁₇ ⁺	484	c	c	
C12 Terpene Acetate Esters						
Isobornyl Acetate	C ₁₂ H ₂₀ O ₂	C ₁₂ H ₂₁ O ₂ ⁺	552	b	4545	0.03
Linalyl Acetate	C ₁₂ H ₂₀ O ₂	C ₁₂ H ₂₁ O ₂ ⁺	592	b	4545	d
Acetone						
Acetone	C ₃ H ₆ O	C ₃ H ₇ O ⁺	64	2.8 x 10 ⁶	8350	0.9

^aUsed an average of camphene and α -terpinene sensitivities (1.2 x 10⁶ cnts ppb⁻¹)

^bNot quantified.

^cUsed 1,8-cineole sensitivity.

^dAmbiguous fH^+ .

The online PTR-MS GC measurements allowed us to quantify the concentrations of all of the monoterpenes and C10 terpene alcohols (linalool and 1,8-cineole) at four different times in Wk1 and once in Wk2. We quantified a maximum concentration of linalyl acetate in the restroom using the real-time PTR-MS signal for $C_{12}H_{21}O_2^+$. For monoterpenes we did not directly calibrate for, ocimene and terpinolene, we estimated sensitivities based on the average sensitivities of camphene and α -terpinene. Using the authentic standards, we were also able to directly calibrate for 1,8-cineole and assumed the sensitivity of linalool was the same. Both linalool and 1,8-cineole were quantified from PTR-MS GC measurements using the $C_{10}H_{17}^+$ ion signal since it was considerably larger than the signal from the ion corresponding to the proton-transfer product $C_{10}H_{19}O^+$.

PTR-MS GC chromatograms for ions corresponding to the protonated monoterpene ion ($C_{10}H_{17}^+$), C10 terpene alcohols ($C_{10}H_{19}O^+$), and C12 terpene acetate esters ($C_{12}H_{21}O_2^+$) are shown in Fig. S2.

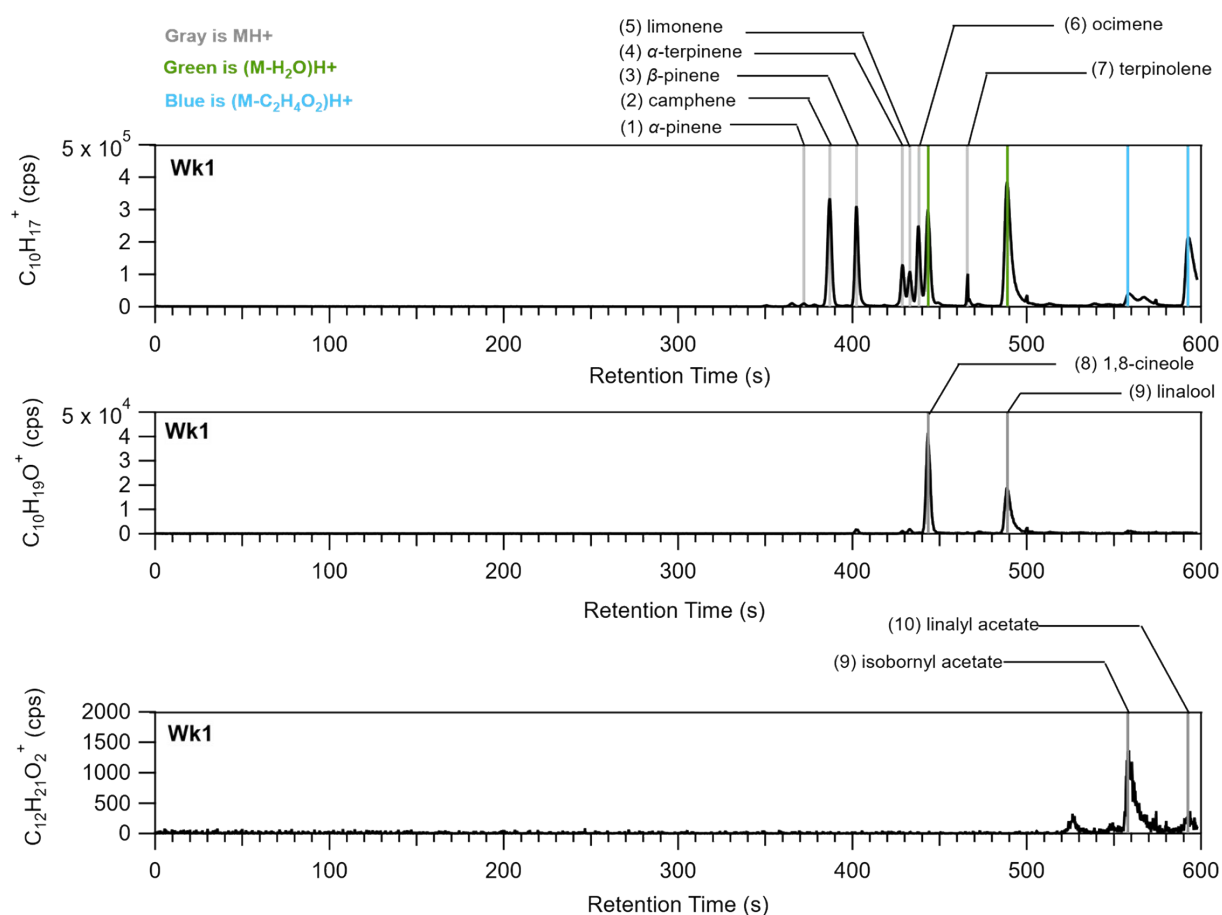


Fig. S2. PTR-MS GC measurement of $C_{10}H_{17}^+$ (top), $C_{10}H_{19}O^+$ (middle), and $C_{12}H_{21}O_2^+$ (bottom). Monoterpenes were identified from retention times measured from standard cylinders. The headspace of a container of linalool was sampled to verify the retention time. The linalyl acetate and isobornyl acetate were assumed based on fragmentation patterns and boiling points.

The $C_{10}H_{17}^+$ ion had not only isomeric interferences from the seven monoterpenes being emitted from the urinal pad, but also from fragments of C10 terpene alcohols and C12 terpene acetate esters. Deconvoluting the contributions of monoterpenes from the real-time PTR-MS $C_{10}H_{17}^+$ ion signal was not feasible.

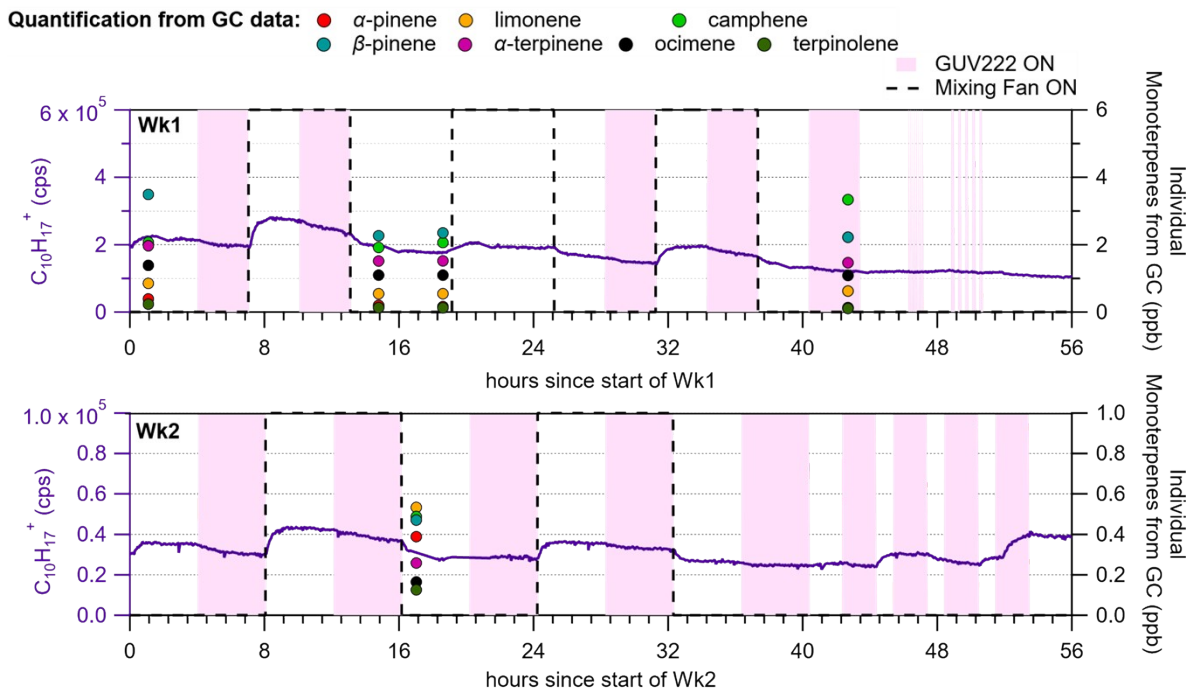


Fig. S3. Time series of the $C_{10}H_{17}^+$ ion signal from the real-time PTR-MS data (left axis) with the speciated monoterpenes quantified from GC measurements (right axis) for Wk1 (top) and Wk2 (bottom). The terpenoids shown in these time series are likely emitted from the urinal pads and thus the real-time measurements go up when the fan is turned on likely because of enhanced emission or from mixing effects. As shown in Fig. S2 the $C_{10}H_{17}^+$ signal in the real-time PTR-MS data is comprised of monoterpene isomers, C10 terpene alcohol dehydration products, and C12 terpene acetate ester fragmentation products. Thus, we do not convert the $C_{10}H_{17}^+$ signal to concentration. Purple shaded region indicates when GUV222 was on and dotted lines indicate when the mixing fan was on.

We did not measure linalyl acetate effectively with the PTR-MS GC so we determined a maximum concentration from the $C_{12}H_{21}O_2^+$ ion measured with real-time PTR-MS (Fig. S4).

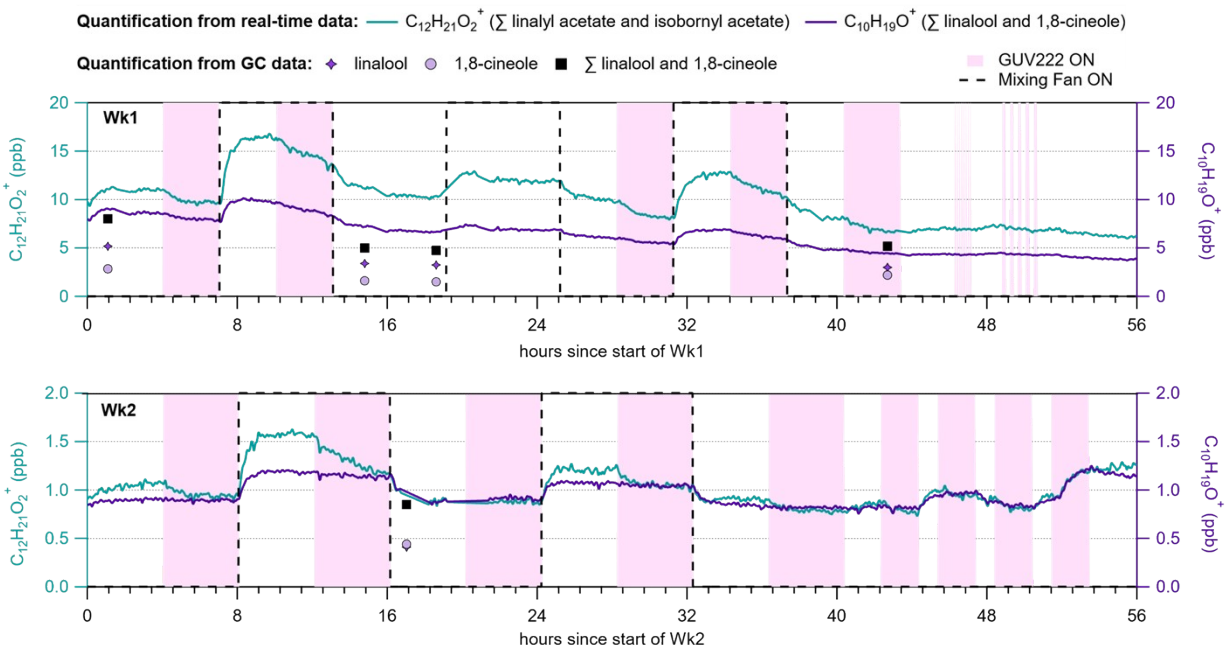


Fig. S4. Time series of C12 Terpene Acetate Ester isomers contributing to the $C_{12}H_{21}O_2^+$ (teal, left axis; linalyl acetate and isobornyl acetate) and C10 Terpene Alcohol isomers contributing to the $C_{10}H_{19}O^+$ PTR-MS ion signals (purple, right axis; 1,8-cineole and linalool) for Wk1 (top) and Wk2 (bottom). In contrast to $C_{10}H_{17}^+$, $C_{10}H_{19}O^+$ and $C_{12}H_{12}O_2^+$ did not have interferences from fragmentation and thus we could convert the real-time signal to concentration. The solid lines are real-time PTR-MS ion signals converted to concentration using a sensitivity of 140 cps ppb^{-1} for $C_{12}H_{12}O_2^+$ and 760 cps ppb^{-1} for $C_{10}H_{19}O^+$. The sensitivity for $C_{12}H_{12}O_2^+$ was calculated from the k_{PTR} versus sensitivity relationship and then corrected for fragmentation (i.e., multiplying original sensitivity of $4500 \text{ cps ppb}^{-1}$ by 0.03 to account for a 3% yield of the H^+ adduct from the reaction of the VOC with H_3O^+). The sensitivity of 1,8-cineole was determined from calibrations and linalool was assumed to have the same sensitivity. Markers show linalool (dark purple, star) and 1,8-cineole (light purple, circle) concentrations calculated from GC measurements. The sum of linalool and 1,8-cineole concentrations determined from GC measurements agree with the $C_{10}H_{19}O^+$ (purple line) on average within 15%. Purple shaded region indicates when GUV222 was on and dotted lines indicate when the mixing fan was on.

We determined the maximum sensitivity for $C_{12}H_{21}O_2^+$ using the relationship between k_{PTR} and sensitivity(*I-3*) parameterized for our instrument as reported elsewhere(*5*). We calculated a maximum sensitivity for $C_{12}H_{21}O_2^+$ of $4500 \text{ cps ppb}^{-1}$, but then corrected this value for the fraction of $C_{12}H_{20}O_2$ that forms $C_{12}H_{21}O_2^+$ after reaction with H_3O^+ compared to the fraction that fragments or forms water clusters (f_{H^+}).

$$f_{H^+} = \frac{[MH]^+}{[MH]^+ + [M(H_2O)H]^+ + [fragments]^+} \quad (\text{S1})$$

where MH^+ is the proton-transfer product for a VOC, $M(H_2O)H^+$ is a water cluster, and fragments are dissociation products of the MH^+ ion. We assume the signals we measure for the various ions are proportional to concentration.

Characterization of product ion distributions from PTR-MS is the subject of an upcoming publication from our group. The f_{H^+} measured for isobornyl acetate was 0.03 for our PTR-MS and we assumed that value was similar to what would be measured for linalyl acetate. Thus, we determined the corrected $C_{12}H_{21}O_2^+$ sensitivity to be 140 cps ppb⁻¹. Converting the $C_{12}H_{21}O_2^+$ real-time ion signal to concentration provides an upper bound limit on the concentration of linalyl acetate because of isomeric interference from isobornyl acetate which was also present in the restroom air.

Differences in PTR-MS GC sample volume occurred during the restroom measurements and so acetone was used as a reference for correcting concentrations of terpenoids measured by PTR-MS GC. Acetone response was demonstrated to be uniform in PTR-MS and PTR-MS GC measurements for our instrument(5), indicating acetone did not breakthrough the thermal desorption tube and could be used as a correcting factor to address varying PTR-MS GC sample volumes. We calibrated directly for acetone during the measurement period and converted the real-time $C_3H_7O^+$ ion signal to concentration. We then quantified acetone from the PTR-MS GC measurements and found acetone was generally lower, compared to real-time quantified acetone, by a factor of 1.5 to 3.0. We applied the factor used to correct GC acetone concentrations to real-time acetone concentrations to all terpenoids quantified from GC data (Table S5).

Table S5. Literature values for O₃ + VOC reaction rate constants used. Average and standard deviation terpenoid concentrations, determined from GC-PTR-MS measurements, and calculated O₃ k_{rxn,VOC}.

Urinal pad VOC	k _{O₃+VOC} [*]	[VOC] (ppb)		O ₃ k _{rxn,VOC} (h ⁻¹)	
		Wk1	Wk2 ^{***}	Wk1	Wk2 ^{***}
Limonene	^a 210	0.64 ± 0.15	0.53	0.012 ± 0.003	0.010
Linalool	^b 430	3.61 ± 1.00	0.44	0.14 ± 0.04	0.017
^{**} Linalyl Acetate	^c 205	< 6	< 1.22	0.13 ± 0.02	0.027
α-terpinene	^d 8,700	1.61 ± 0.23	0.26	1.3 ± 0.2	0.202
Ocimene	^e 385	1.16 ± 0.15	0.16	0.037 ± 0.005	0.005
α-pinene	^f 84	0.22 ± 0.12	0.39	0.002 ± 0.001	0.003
β-pinene	^f 19	2.56 ± 0.61	0.47	0.004 ± 0.001	0.001
Terpinolene	^d 1,400	0.15 ± 0.06	0.13	0.02 ± 0.01	0.016
Camphene	^g 0.9	2.35 ± 0.66	0.49	---	---

^{*}k_{O₃+VOC} for 298K, units (x10⁻¹⁸ cm³ molecule⁻¹ s⁻¹)

^{**}Quantified from real-time PTR-MS measurements.

^{***}Only one PTR-MS GC measurement available.

^aShu and Atkinson (1994)

^bBernard, et al. (2012)

^ck_{O₃+VOC} estimated from linalyl acetate O₃ oxidation data in Destailhats, et al. (2006) with a rate constant approximately half that of linalool

^dWitter, et al. (2002)

^eKim, et al. (2011)

^fAtkinson, et al. (1990a)

^gAtkinson, et al. (1990b)

2. Differences in particle production dynamics from GUV222 with and without the use of a mixing fan.

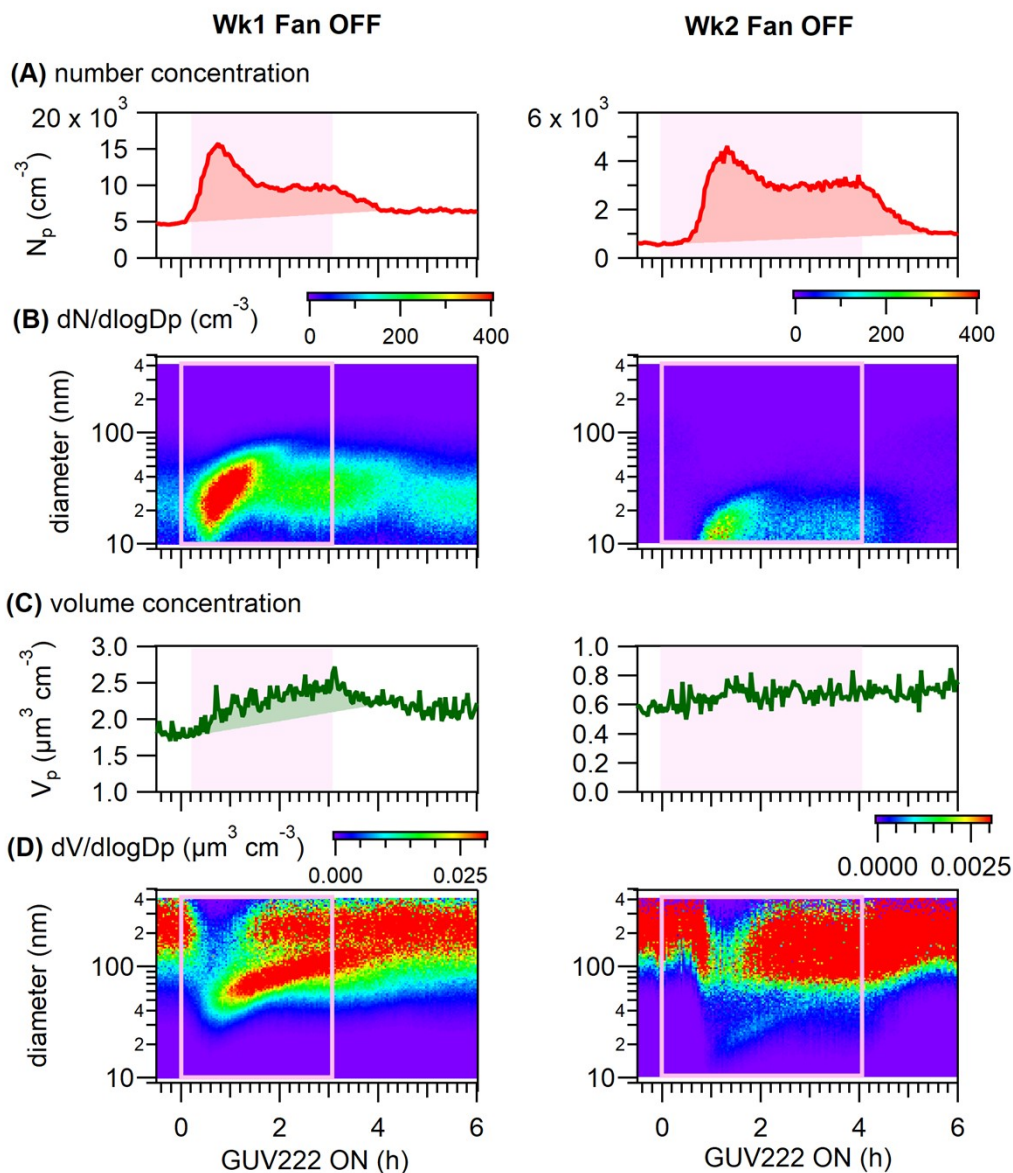


Fig. S5. Particle production dynamics when a mixing fan is not used (OFF) while GUV222 is on in a restroom during Weekend 1 (left) and Weekend 2 (right). Shaded regions indicate when GUV222 is on. Filled in areas for number and volume concentrations indicate the amount of byproduct produced from GUV222. (A) Particle number concentrations, N_p . (B) N_p size distributions. Boxes indicate when GUV222 is on. (C) Particle volume concentrations (V_p). (D) V_p size distributions.

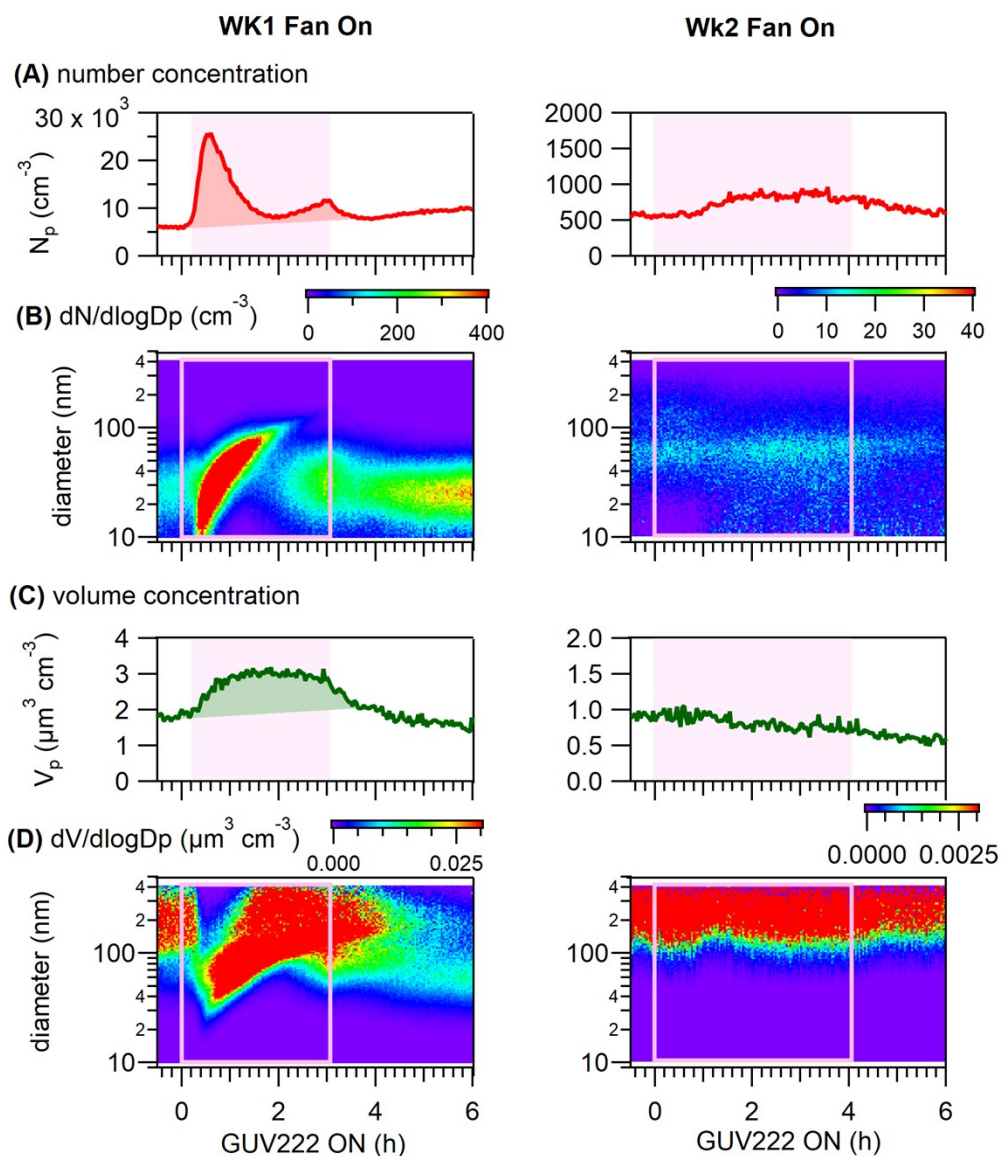


Fig. S6. Particle production dynamics when a mixing fan is used (ON) while GUV222 is on in a restroom during Weekend 1 (left) and Weekend 2 (right). All the details for Fig. S5 apply to this figure. The image color scale for panels B and D are an order of magnitude smaller for Wk2 compared to Wk1. The y-axis ranges for panels A and C are lower for Wk2 compared to Wk1.

3. Measurements of air change rates (ACR).

We measured air change rates (ACR) by fitting Equation S2 to time periods of acetone concentration decay for Wk1 and SF₆ signal decay for Wk2 (Fig. S7) measured by the time-of-flight proton-transfer mass spectrometer (PTR-MS),

$$[X]_t = [X]_{t=1.5h} + ([X]_{t=0h} - [X]_{t=1.5h})e^{-ACR \cdot t} \quad (S2)$$

where X is either acetone or SF₆.

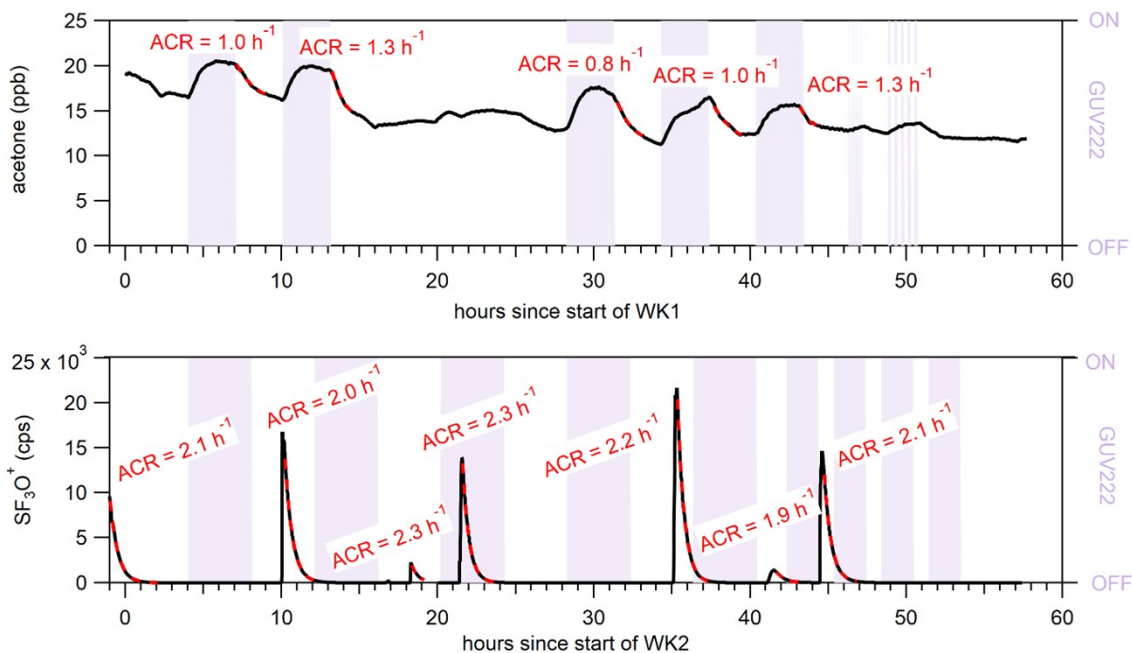


Fig. S7. Determination of ACRs for Wk1 (top) and Wk2 (bottom) using acetone and SF₆ as inert tracers.

We quantify acetone from the C₃H₇O⁺ ion signal and measure SF₆ from the SF₃O⁺ ion signal. Inert gases like CO₂, SF₆, N₂O, etc. are generally recommended for tracer gas dilution test determinations of ACRs, but in Wk1 we did not have a remote system for injecting inert gases into the restroom to measure the ACR. Instead, for Wk1 we use acetone, generated by GUV222, as a practically inert tracer for the ACR determination. Acetone was generated from GUV222 and was observed to decay to background concentrations after the lamps were turned off. We assume that acetone has negligible loss and partitioning to walls. We compared the ACRs determined from the decay of acetone with ACRs determined from injections of SF₆ to the restroom in preliminary experiments. ACRs determined with acetone, on average, agreed within 20 % of those determined from SF₆ decay in the prior weekend.

For Wk2 SF₆ was injected seven times into the restroom to provide a tracer gas dilution measurement of the ACR. Ultra-zero air (UZA) flowed at 1 liter per minute through a 3.1 mm (1/8") Teflon sample line one minute prior to the SF₆ injection. Two liters of 5 % SF₆ in nitrogen

was collected in a gas-tight syringe and delivered to the UZA carrier gas flow for injection into the restroom. UZA flow was turned off one minute after SF₆ injection.

4. O₃ k_{loss,VOC} speciated by terpenoid.

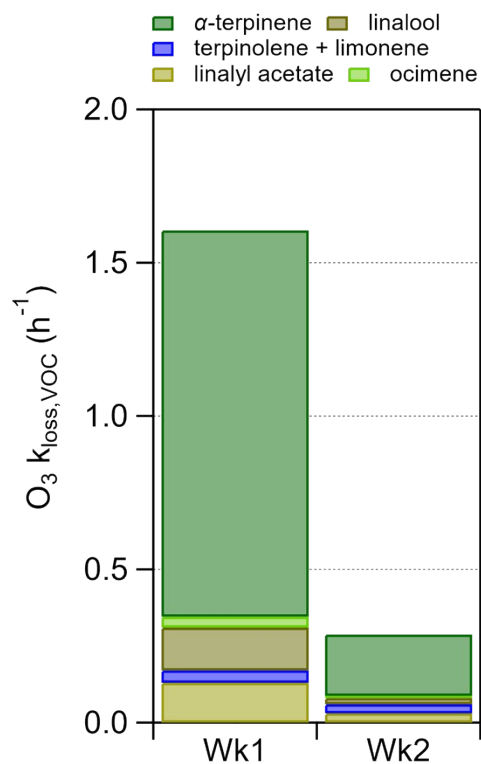


Fig. S8. Contribution of speciated terpenoids to average O₃ k_{loss,VOC}. α-pinene and β-pinene made negligible contributions to O₃ k_{loss,VOC} both weekends and thus are not shown here.

5. Comparison of O₃ production measured in the restroom compared to previous chamber study.

Following an ASTM draft test method for the chemical assessment of air cleaning technologies we reported an O₃ generation rate (GR_{O₃}) of 1220 μg h⁻¹ measured from a single lamp in a 31.5 m³ environmentally-controlled chamber.(11) In the restroom we measured a per lamp GR_{O₃} of 930 μg h⁻¹ ± 110 μg h⁻¹ averaged between the two weekends. We measured small differences in the radial distribution of the irradiance from each of the three lamps (Fig. S9). We expect some of the light from the three lamps in the restroom was attenuated by walls or the restroom stall partitions resulting in a lower GR_{O₃} measured in the restroom compared to the chamber.

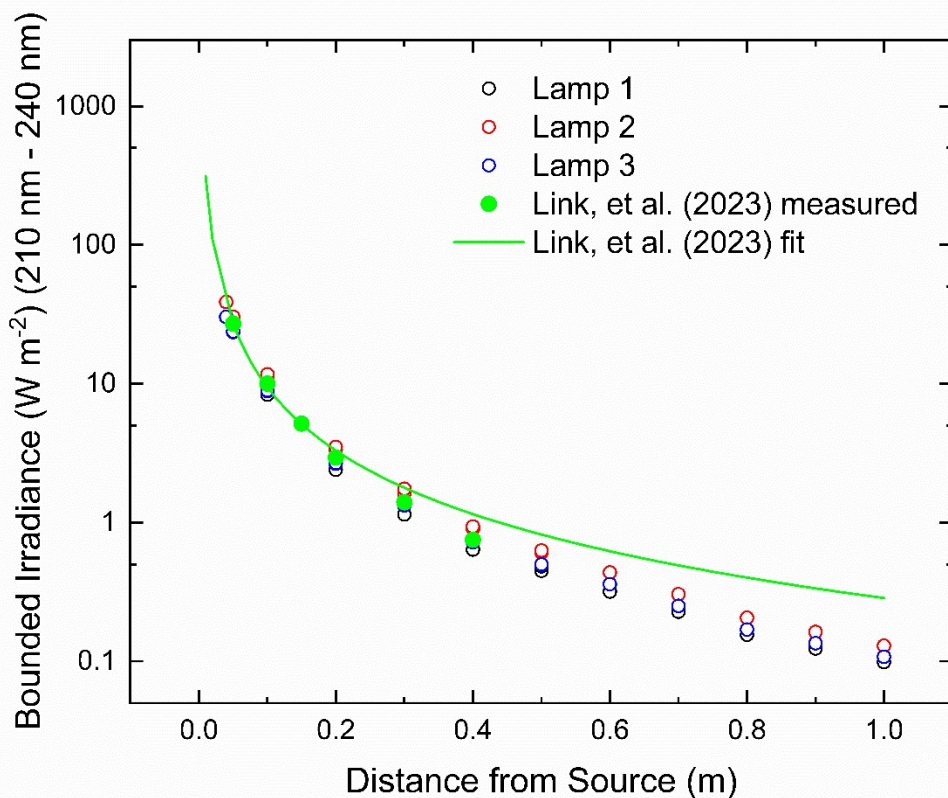


Fig. S9. Comparison of the total irradiance, measured between 210 nm and 240 nm for the three lamps. The green filled dots show a comparison with a measurement of the total irradiance from Lamp 3 six months before the restroom study. The $1/r^2$ is the previously reported fit for the 2/2023 data.

6. Modeling of O₃ in the restroom.

O₃ concentrations were measured in both the restroom and the hallway during the study. Thus, we can use a mass-balance shown in Equation 1 in the main text (Equation S3 here) to predict O₃ concentrations in the restroom from hallway concentrations.

$$[O_3]_{rest,t} = [O_3]_{rest,0} e^{-k_{O_3\text{ removal}}t} + \frac{\left(\frac{N_{lamp} E_{r, O_3}}{V} + [O_3]_{hall} \cdot ACR\right)}{k_{O_3\text{ removal}}} (1 - e^{-k_{O_3\text{ removal}}t}) \quad (S3)$$

We used measurements of hallway O₃ ([O₃]_{hall}), the air change rate (ACR), the number of GUV222 lamps (N_{lamp} = 3), and the volume (V, 59 m³) of the restroom to calculate O₃ concentrations in the restroom ([O₃]_{rest,t}). k_{O₃ removal} was calculated from the mass-balance.

We determine GR_{O₃} and k_{O₃ removal} from Equation S3 by minimizing the absolute value of the difference between measured and predicted O₃ in the restroom,

$$X(t) = |[O_3]_{rest,measured}(t) - [O_3]_{rest,predicted}(t)| \quad (S4)$$

where X(t) is the time-dependent function representing the absolute difference between measured and predicted O₃ concentrations in the restroom. We use an optimization solver to minimize the sum of X(t).

As discussed in the main text, k_{O₃ removal} is the sum of all contributing loss processes to the total first-order rate constant for O₃ removal.

$$k_{O_3\text{ removal}}(t) = k_{loss, surface} + k_{loss, NO}(t) + k_{loss, VOC}(t) + ACR \quad (S5)$$

The time-dependent k_{loss,NO} is determined by multiplying the bimolecular rate constant for the reaction of NO with O₃ (k_{NO+O₃} ≈ 1.9 x 10⁻¹⁴ cm³ molecules⁻¹ s⁻¹ at 298 K)(12) with the NO concentration (molecules cm⁻³) measured in the restroom at each timepoint.

$$k_{loss,NO}(t) = k_{NO+O_3} \cdot [NO]_{restroom}(t) \quad (S6)$$

The time-dependent contribution of terpenoid + O₃ reactions to k_{loss,VOC} is represented as,

$$k_{loss,VOC}(t) = \sum (k_{VOC,i+O_3} \cdot [VOC]_i(t)) \quad (S7)$$

where i denotes an individual terpenoid, k_{VOC+O₃} is the bimolecular rate constant for the reaction of O₃ and a terpenoid (cm³ molecules⁻¹ s⁻¹), and [VOC] is the terpenoid concentration in the restroom (molecules cm⁻³).

We calculated k_{loss,VOC} from four GC measurements in Wk1 and one GC measurement in Wk2. We could see from the real-time measurements of C₁₀H₁₇⁺ that terpenoid, and likely k_{loss,VOC},

increased whenever the fan was on. The $C_{10}H_{17}^+$ signal is composed of multiple terpenoids that have varying reaction constants with ozone. To deconvolute the real time $C_{10}H_{17}^+$ signal into its components, GC measurements were taken four times in Wk1 and once in Wk2 (Fig. S10). This allowed the calculation of the $k_{\text{loss,VOC}}$ at those points in time as shown in Equation S7. To get a time-dependent $k_{\text{loss,VOC}}$ we scale a reference $k_{\text{loss,VOC}}$ calculated from GC measurements in Wk1 and the only calculation of $k_{\text{loss,VOC}}$ from GC measurements in Wk2 by the $C_{10}H_{17}^+$ signal measured from real-time PTR-MS in the respective weekends.

$$k_{\text{loss,VOC}}(t) = k_{\text{loss,VOC,GC,t = reference time}} \cdot \frac{C_{10}H_{17}^+(t)}{C_{10}H_{17,t = \text{reference time}}^+} \quad (\text{S8})$$

For Wk1, the reference value was chosen to be the first GC measurement.

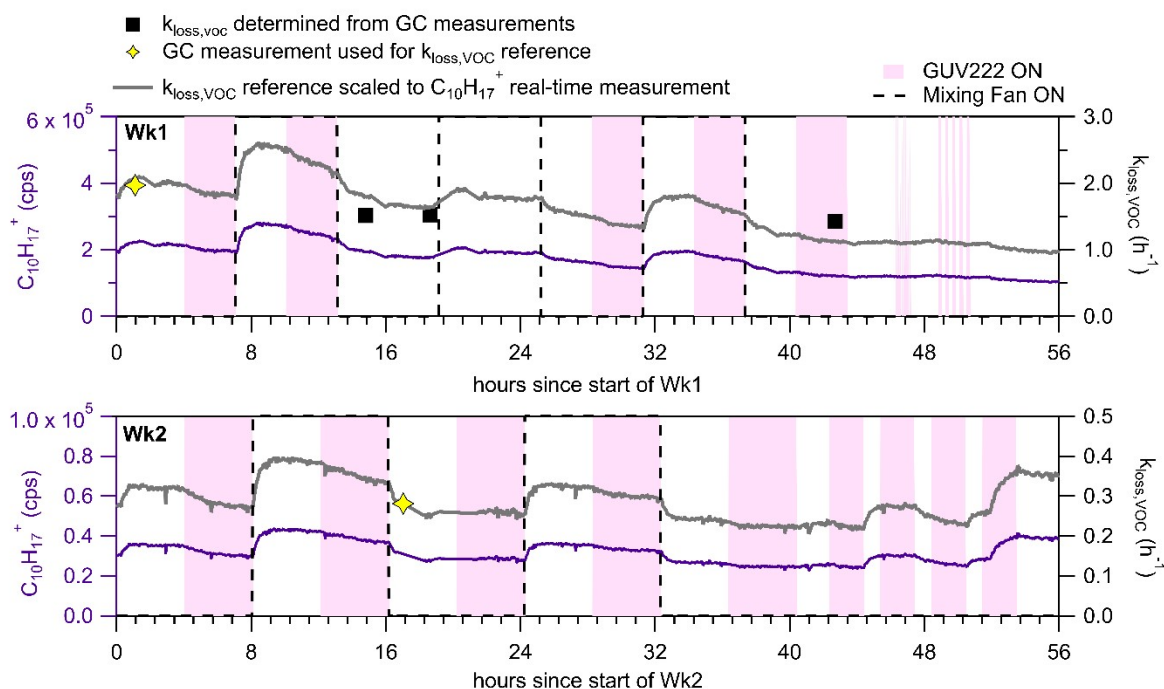


Fig. S10. Scaling of $k_{\text{loss,VOC}}$ calculated at discrete times from GC measurements of terpenoids to the $C_{10}H_{17}^+$ ion signal (counts per second, cps) measured by the real-time PTR-MS.

Because we only measured the ACR at select times during both Wk1 and Wk2 we use the average of the ACR measurements in the respective weeks to constrain the mass-balance minimization (Wk1 ACR = 1.1 h^{-1} and Wk2 ACR = 2.1 h^{-1}).

We minimize Equation S4 using $k_{\text{loss,surface}}$ and GR_{O_3} as the free variables. In other words, the solver varies the values of $k_{\text{loss,surface}}$ and GR_{O_3} until a local minimum in a solution set defined by Equation S3 is determined. For Wk1 we calculated a $k_{\text{loss,surface}}$ of 1.5 h^{-1} . We found that in Wk2 the operation of the mixing fan increased $k_{\text{loss,surface}}$ and thus we calculated a $k_{\text{loss,surface}}$ of 1.7 h^{-1} when the fan was off and 2.4 h^{-1} when the fan was on.

The value of GR_{O_3} calculated from Equation S3 for Wk1 was $850 \mu\text{g h}^{-1}$ and for Wk2 was $1000 \mu\text{g h}^{-1}$. For steady-state calculations we use an average of the two weekends of $930 \mu\text{g h}^{-1} \pm 110 \mu\text{g h}^{-1}$. Model-predicted O_3 concentrations are shown below with measurements in Fig. S11 and S12. Model predicted and measured O_3 agreed within 1.5 ppb for both weekends.

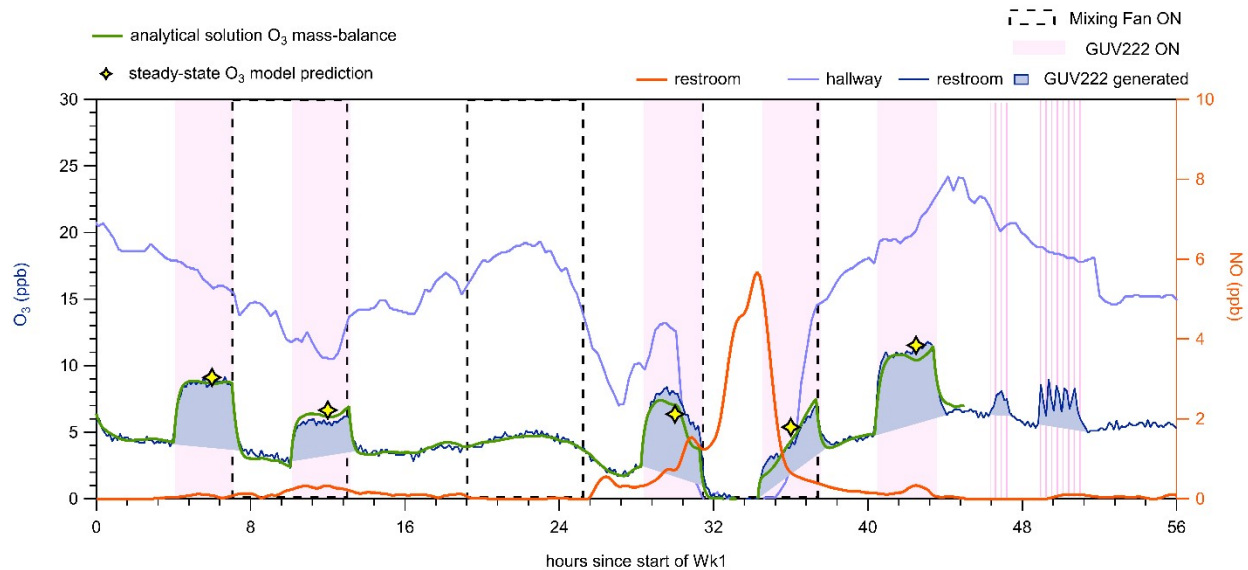


Fig. S11. Model-predicted (green) and measured O_3 in Wk1. O_3 concentrations determined from the steady-state calculation are shown as star markers.

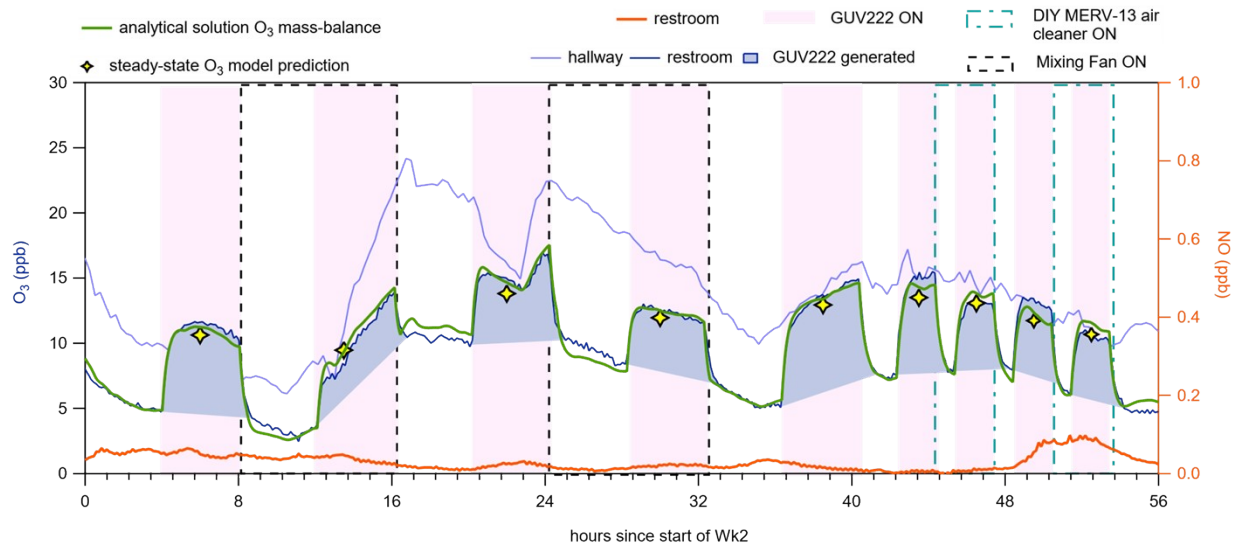


Fig. S12. Model-predicted and measured O_3 in Wk2.

Table S6. Summary data for O₃ loss.

First weekend (Wk2)										
Measurements				Calculated			Steady-State Ozone Loss Analysis (GUV222 ON – OFF)			
GUV222 cycle	ACR (h ⁻¹) [§]	Δ[O ₃] from GUV222 (ppb)	O ₃ k _{NO} (h ⁻¹)	O ₃ k _{VOC} (h ⁻¹)	O ₃ k _{loss} (h ⁻¹)	k _{surface} (h ⁻¹)	[O ₃] gas-phase (ppb)	O ₃ Loss VOCs (ppb)	O ₃ Loss Surface (ppb)	ΔO _{3,loss} GUV222 (ppb)
1	1.1	5.1	0.1	1.9	4.6	1.5	5.3	9.0	7.2	16.2
2*	1.3	3.1	0.4	2.3	5.4	1.5	4.5	9.5	6.6	16.1
3	0.8	2.8	1.7	1.4	5.7	1.5	4.2	5.4	5.8	11.2
4*	1.0	3.9	0.9	1.6	5.2	1.5	4.6	6.9	6.8	13.7
5	1.3	5.3	0.3	1.2	4.0	1.5	6.0	6.3	8.2	14.6
Average ± Std. deviation	1.1 ± 0.2	4.1 ± 1.1	0.7 ± 0.7	1.7 ± 0.5	5.0 ± 0.7	1.5	4.9 ± 0.7	7.4 ± 1.8	6.9 ± 0.9	14.3 ± 2.1
Second Weekend (Wk2)										
Measurements				Calculated			Steady-State Ozone Loss Analysis (GUV222 ON – OFF)			
GUV222 cycle	ACR (h ⁻¹) [§]	Δ[O ₃] from GUV222 (ppb)	O ₃ k _{NO} (h ⁻¹)	O ₃ k _{VOC} (h ⁻¹) ^{**}	O ₃ k _{loss} (h ⁻¹)	k _{surface} (h ⁻¹)	[O ₃] gas-phase (ppb)	O ₃ Loss VOCs (ppb)	O ₃ Loss Surface (ppb)	ΔO _{3,loss} GUV222 (ppb)
1	2.1	7.0	0.1	0.3	4.3	1.7	5.7	0.8	4.9	5.7
2*	2.0	4.4	0.1	0.4	5.0	2.4	4.8	0.8	5.8	6.6
3	2.4	5.0	> 0.1	0.3	4.2	1.7	5.8	0.7	5.0	5.7
4*	2.3	4.7	> 0.1	0.3	4.9	2.4	4.9	0.7	5.9	6.6
5	2.2	7.5	> 0.1	0.2	4.2	1.7	5.8	0.6	5.0	5.6
6	1.9	7.5	> 0.1	0.2	4.1	1.7	5.9	0.6	5.0	5.7
7*	2.2	5.1	> 0.1	0.3	4.2	1.7	5.8	0.8	5.0	5.7
8	2.2	5.7	0.1	0.2	4.2	1.7	5.8	0.6	4.9	5.6
9*	2.2	5.0	0.1	0.3	4.3	1.7	5.6	0.8	4.8	5.6
Average ± Std. deviation	2.2 ± 0.2	5.6 ± 1.1	0.1 ± 0.1	0.3 ± 0.1	4.0 ± 0.6	0.8 ± 0.1	5.6 ± 0.4	0.7 ± 0.1	5.1 ± 0.4	5.9 ± 0.4

*Mixing fan or DIY air cleaner on.

§Average ACR was used for O₃ modeling.

7. Example ocimene O₃ oxidation mechanism producing select VOC_{O₃ Ox.} byproducts.

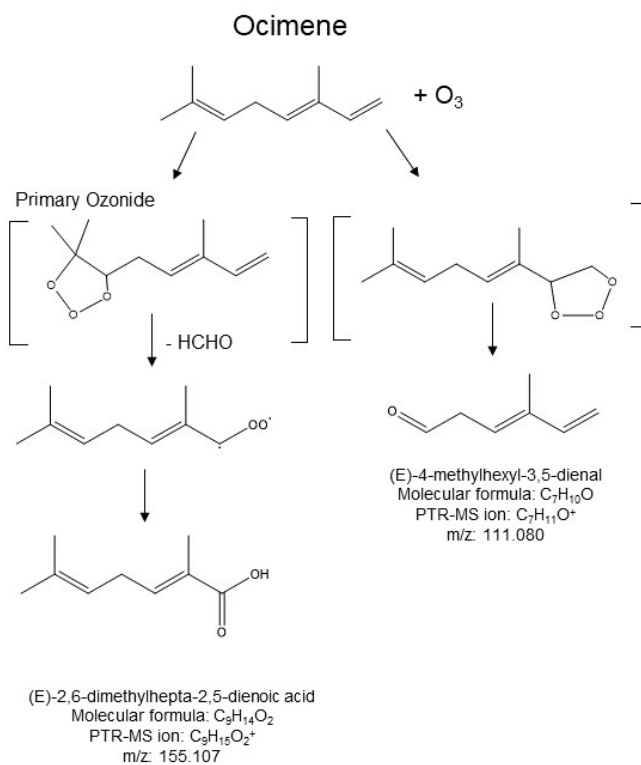


Fig. S13. Example mechanism of ocimene oxidation by O₃ (adopted from Touhami, et al. (2024)).(13) O₃ reacts with the double bonds on ocimene to form primary ozonide intermediates that decompose to form stable products.

8. Deposition efficiency of respired particles in three zones of the respiratory tract as a function of particle diameter.

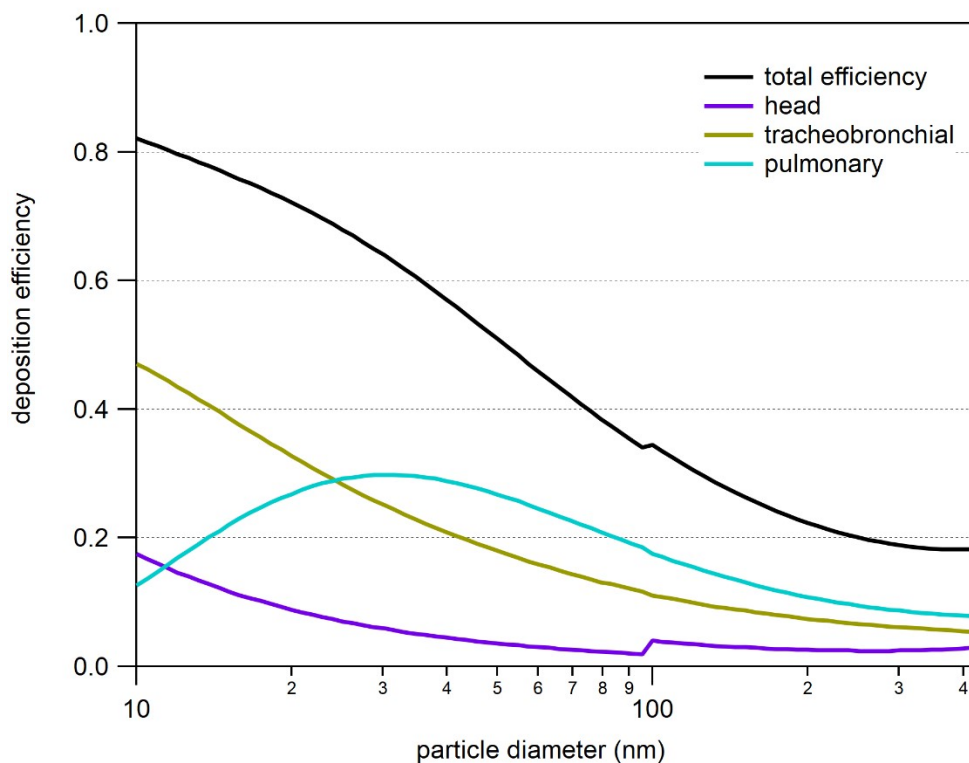


Fig. S14. Inhaled particle deposition efficiencies calculated from an open-source multiple-path particle deposition open-source software.

9. Estimation of $\text{VOC}_{\text{cond,g}}$ wall loss rate constant ($k_{\text{cond,w}}$) and expected ranges for $f_{\text{cond,p}}$

We estimate the loss rate constant for VOC_{cond} condensing to walls, $k_{\text{cond,w}}$, using the parameterization of McMurry and Grosjean (1985)(14) determined by assuming steady-state, diffusion-limited mass transport of a condensing species (accommodation coefficient equal to 1),

$$k_{\text{cond,w}} = \frac{A}{V} \frac{2}{\pi} \sqrt{D_g \cdot k_e} \quad (\text{S9})$$

where A/V is the surface area to volume ratio of the restroom (2.5 m^{-1}), D_g is the gas diffusion coefficient of a low-volatility monoterpene oxidation product with a molecular weight of 200 g mol^{-1} (16) ($D_g = 7.0 \times 10^{-6} \text{ m}^2 \text{ s}^{-1}$), and k_e is the coefficient of eddy diffusion (s^{-1}). The choice of k_e can have a pronounced impact on the $k_{\text{cond,w}}$ estimate. We show below in Fig. S15 the relationship of $k_{\text{cond,w}}$ to k_e as a function of D_g (inversely proportional to the square root of the molecular weight through Graham's Law) across a range of five plausible k_e values reported in Charan et al. (2019).

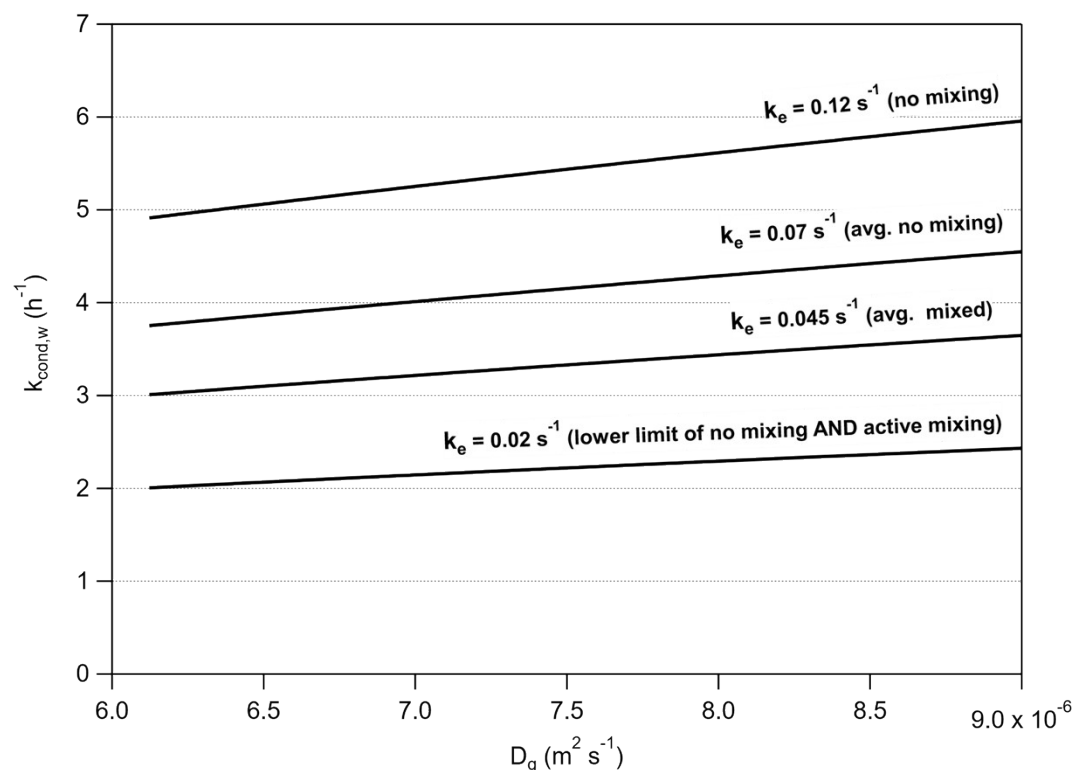


Fig. S15. $\text{VOC}_{\text{cond,g}}$ wall-loss rate constant ($k_{\text{cond,w}}$) versus gas-phase diffusion coefficient (D_g). Each line is calculated from using a different k_e value with ranges estimated from Teflon chambers that were and were not actively mixed as reported in Charan et al. (2019).(17)

To the best of our knowledge, no empirical determinations of k_e have been published for real indoor spaces. We rely on measurements of k_e performed in Teflon environmental chambers (14, 17-19) to constrain our estimate of $k_{\text{cond,w}}$. Following Brune (2019) we calculate k_e as a function of the restroom volume (V),

$$k_e = 0.004 + 10^{-2.25} \cdot V^{0.75} \quad (\text{S10})$$

We calculate a k_e of 0.12 s^{-1} in the 59 m^3 restroom. Zhang et al. (2014) reported ranges of k_e in actively mixed chambers (using a mixing fan) of 0.02 s^{-1} to 0.12 s^{-1} and chamber without active mixing of 0.015 s^{-1} to 0.075 s^{-1} . Considering the ranges of k_e provided by Zhang et al. (2014) in chambers with and without active mixing, we do not expect to see changes in k_e in the restroom with and without fan mixing substantive enough to increase an already large $k_{\text{cond,w}}$. We calculate a $k_{\text{cond,w}}$ of 5.44 h^{-1} for this study. This value is approximately more than five times higher than the ACR in Wk1 and more than two times higher than the ACR in Wk2 and because vapor wall losses are already pronounced, we expect it would be difficult to measure any increase in wall loss efficiency induced by active mixing. Fig. S16 shows that going from a k_e of 0.12 s^{-1} to 0.02 s^{-1} the $f_{\text{cond,p}}$ (i.e., fraction of $\text{VOC}_{\text{cond,g}}$ lost to condensation to aerosol) increases from 0.108 to 0.187 for Wk1 and 0.023 to 0.040 for Wk2.

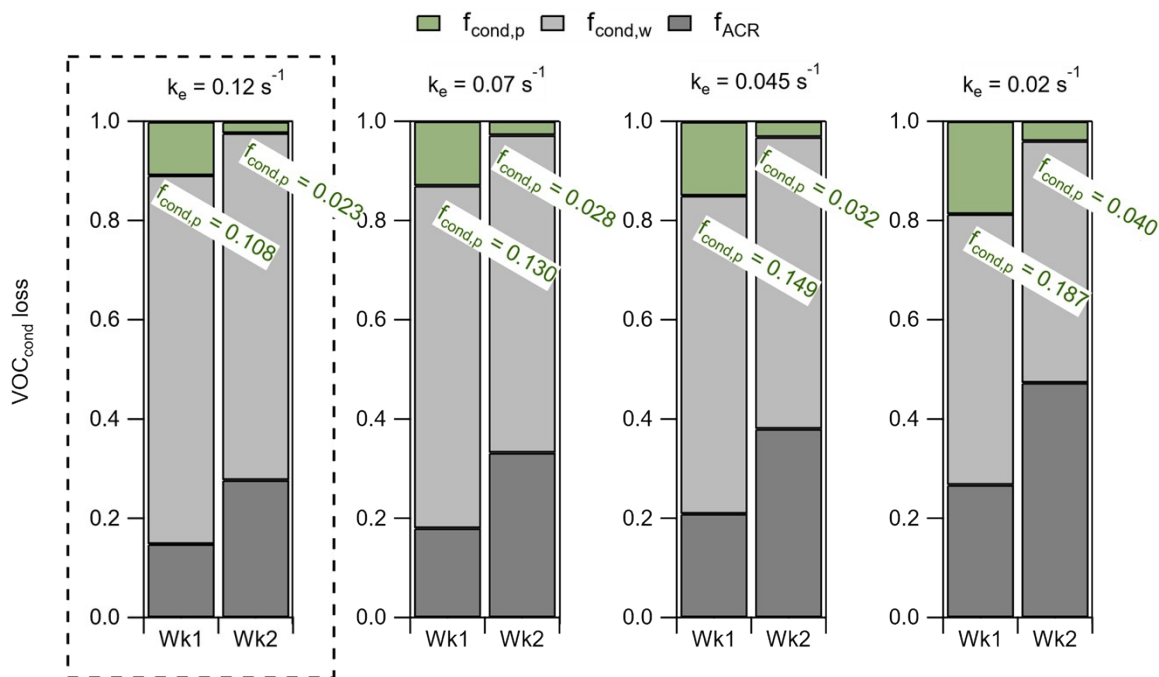


Fig. S16. Sensitivity of $\text{VOC}_{\text{cond,g}}$ losses to the range of k_e shown in Fig. S15. $f_{\text{cond,p}}$ for both Wk1 and Wk2 increase by approximately 80 %, or an absolute fraction of 0.079 (Wk1) to 0.017 (Wk2), when going from a high k_e value of 0.12 s^{-1} to a low value of 0.02 s^{-1} . The dashed box indicates the k_e that was used for the $\text{VOC}_{\text{cond,g}}$ loss calculations in this study.

Equation 13 in the main text includes the semi-empirical Fuchs–Sutugin correction for gas diffusion to a particle surface in the transition regime(21) (β) calculated as:

$$\beta = \frac{0.75\alpha \cdot (1 + Kn)}{Kn^2 + Kn + 0.283Kn \cdot \alpha + 0.75\alpha} \quad (\text{S11})$$

where α is the sticking probability (also known as the mass accommodation coefficient, dimensionless value between 0 and 1; assumed equal to 1 in this study) of $\text{VOC}_{\text{cond,g}}$ to a surface or aerosol and Kn is the Knudsen number (dimensionless).

$$Kn = \frac{\lambda_{AB}}{R_p} \quad (\text{S12})$$

λ_{AB} is the mean free path of a gas (6×10^{-9} m for standard conditions) and R_p is the particle radius (m).

Table S7. Summary data for O_3 loss and M_p used to construct Figure 8 in the main text.

First weekend (Wk1)						
GUV222 cycle	$\Delta[\text{O}_3]_{\text{loss,VOC,GUV222}}$ (ppb)	Measured M_p ($\mu\text{g m}^{-3}$)	$f_{\text{cond,p}}$	$f_{\text{cond,p}} \cdot M_p$ ($\mu\text{g m}^{-3}$)	Measured ΔM_p ($\mu\text{g m}^{-3}$)	Measured Y_{M_p}
1	9.0	4.64	0.24	1.10	2.60	0.29
2*	9.5	3.71	0.10	0.37	2.39	0.25
3	5.4	3.75	0.08	0.30	1.88	0.35
4*	6.9	3.37	0.04	0.14	1.10	0.16
5	6.3	3.40	0.08	0.27	0.68	0.11
Second weekend (Wk2)						
GUV222 cycle	$\Delta[\text{O}_3]_{\text{loss,VOC,GUV222}}$ (ppb)	Measured M_p ($\mu\text{g m}^{-3}$)	$f_{\text{cond,p}}$	$f_{\text{cond,p}} \cdot M_p$ ($\mu\text{g m}^{-3}$)	Calculated ΔM_p ($\mu\text{g m}^{-3}$)**	Calculated Y_{M_p} ***
1	0.8	1.54	0.04	0.06	0.13	0.17
2*	0.8	1.41	0.02	0.03	0.07	0.09
3	0.7	3.74	0.03	0.10	0.20	0.28
4*	0.7	1.48	0.01	0.02	0.04	0.06
5	0.6	0.86	0.02	0.02	0.03	0.05
6	0.6	1.14	0.02	0.02	0.03	0.06
7*	0.8	0.89	0.02	0.02	0.04	0.05
8	0.6	1.33	0.03	0.04	0.08	0.13
9*	0.6	0.76	0.02	0.03	0.02	0.04

*Mixing fan on or DIY air cleaner on.

**Calculated from Equation 11 in main text.

***Calculated from Equation 15 in the main text.

10. Prediction of M_p production from speciated terpene reactions and secondary organic aerosol yields

We compared M_p concentrations produced by GUV222 in Wk1 to predictions using measured terpene concentrations and a secondary organic aerosol yield (Y_{SOA}) calculation. Literature values we used for Y_{SOA} in our calculation are shown in Table S8. We consider this calculation as a rough approximation of the M_p we might expect to be produced as measurements Y_{SOA} vary considerably depending on if an OH scavenger is used, NO concentrations, and the relative humidity.

M_p production from GUV222 ($\Delta M_{p,predict}$) can be predicted if the amount of precursor VOC consumed by O_3 (ΔC) can be measured and the terpene-specific Y_{SOA} is known following Equation S17,

$$\Delta M_{p,predict} = \Delta C \cdot Y_{SOA,terpene} \cdot f_{cond} \quad (S13)$$

ΔC can be determined assuming a constant O_3 concentration (i.e., the concentration of O_3 measured at steady-state when GUV222 was on) following Equation S18,

$$\Delta C = C_{final} - C_0 \quad (S14)$$

During Wk1 we can reasonably estimate the starting concentrations (C_0) from GC measurements. However, we only took four GC measurements which allowed us to quantify individual monoterpene concentrations and, thus, could not measure C_{final} for each on/off cycle. To calculate C_{final} for all the monoterpenes during the GUV222 on/off cycles we constrain the time it takes for the terpene + O_3 reaction to reach steady-state (t_{rxn}) in Equation S19 using the C_{final} measured for linalool,

$$C_{final} = C_0 e^{-k_{O_3+VOC} [O_3]_{ss} \cdot t_{rxn}} \quad (S15)$$

where k_{O_3+VOC} is the bimolecular rate constant for the monoterpene reaction with O_3 ($\text{cm}^3 \text{molecules}^{-1} \text{s}^{-1}$) and $[O_3]_{ss}$ is the steady-state concentration of O_3 measured from the GUV222 on cycle. This calculation of ΔC assumes during the GUV222 on/off cycle that the emission rate of the terpene from the urinal pad, loss via air change, and any influence of surface sorption processes are constant.

We quantified the $C_{10}H_{19}O^+$ ion signal from PTR-MS real-time measurements using the sensitivity measured for 1,8-cineole (Table S4). The $C_{10}H_{19}O^+$ ion includes contributions from both 1,8-cineole and linalool. When GUV222 was on we would observe a decrease in the $C_{10}H_{19}O^+$ concentration (as measured from the real-time PTR-MS data). Because linalool is reactive to O_3 ($k_{O_3+linalool} = 4.6 \times 10^{-16} \text{ cm}^3 \text{ molecules}^{-1} \text{ s}^{-1}$) and 1,8-cineole is much less reactive ($k_{O_3+1,8-cineole} = 1 \times 10^{-19} \text{ cm}^3 \text{ molecules}^{-1} \text{ s}^{-1}$) we assume the ΔC measured for $C_{10}H_{19}O^+$ is all from linalool reacting. We then subtract linalool ΔC (measured from the real-time PTR-MS data)

from C_0 (from the PTR-MS GC data) to get C_f and use Equation S7 to determine the t_{rxn} needed for C_0 to react to C_f given the $[O_3]_{ss}$. We then use Equation S7, with the t_{rxn} constrained by linalool reaction, to determine the ΔC for each of the monoterpenes included in our M_p production calculation. All the values used in our calculation are presented in Table S8.

Table S8. Values used for estimating M_p production from Y_{SOA} and reacted monoterpenes.

Wk1 ON/OFF Cycles							
	Linalool	Ocimene	α -terpinene	β -pinene	α -pinene	Limonene	Terpinolene
Y_{SOA}^a	0.01	0.05	0.50	0.32	0.20	0.20	0.20
Cycle 1 ($f_{cond} = 0.27$, $[O_3]_{ss} = 5.0$ ppb, $t_{rxn} = 0.7$ h)							
	Linalool	Ocimene	α -terpinene	β -pinene	α -pinene	Limonene	Terpinolene
C_0 ($\mu\text{g m}^{-3}$)	33.60	8.00	11.35	20.21	2.25	4.90	1.33
ΔC ($\mu\text{g m}^{-3}$)	3.74	0.84	10.42	0.12	0.06	0.32	0.48
$\Delta M_{p,predict}$ ($\mu\text{g m}^{-3}$)	0.010	0.011	1.41	0.011	0.003	0.017	0.026
Total	$\Delta M_{p,predict} = 1.46 \mu\text{g m}^{-3}$			$\Delta M_{p,measured} = 2.60 \mu\text{g m}^{-3}$			
Cycle 2 ($f_{cond} = 0.17$, $[O_3]_{ss} = 3.1$ ppb, $t_{rxn} = 1.2$ h)							
	Linalool	Ocimene	α -terpinene	β -pinene	α -pinene	Limonene	Terpinolene
C_0 ($\mu\text{g m}^{-3}$)	41.65	9.15	13.61	23.16	2.90	5.79	2.03
ΔC ($\mu\text{g m}^{-3}$)	4.44	0.97	12.52	0.14	0.08	0.38	0.73
$\Delta M_{p,predict}$ ($\mu\text{g m}^{-3}$)	0.008	0.008	1.064	0.008	0.003	0.013	0.025
Total	$\Delta M_{p,predict} = 1.10 \mu\text{g m}^{-3}$			$\Delta M_{p,measured} = 2.39 \mu\text{g m}^{-3}$			
Cycle 3 ($f_{cond} = 0.13$, $[O_3]_{ss} = 3.9$ ppb, $t_{rxn} = 1.6$ h)							
	Linalool	Ocimene	α -terpinene	β -pinene	α -pinene	Limonene	Terpinolene
C_0 ($\mu\text{g m}^{-3}$)	22.79	6.37	8.67	13.61	1.16	3.18	0.75
ΔC ($\mu\text{g m}^{-3}$)	4.34	1.13	8.42	0.14	0.05	0.35	0.41
$\Delta M_{p,predict}$ ($\mu\text{g m}^{-3}$)	0.006	0.007	0.560	0.006	0.001	0.009	0.011
Total	$\Delta M_{p,predict} = 0.59 \mu\text{g m}^{-3}$			$\Delta M_{p,measured} = 1.10 \mu\text{g m}^{-3}$			
Cycle 4 ($f_{cond} = 0.15$, $[O_3]_{ss} = 5.3$ ppb, $t_{rxn} = 0.6$ h)							
	Linalool	Ocimene	α -terpinene	β -pinene	α -pinene	Limonene	Terpinolene
C_0 ($\mu\text{g m}^{-3}$)	19.53	6.31	8.45	12.74	0.75	3.59	0.58
ΔC ($\mu\text{g m}^{-3}$)	1.90	0.57	7.52	0.07	0.02	0.20	0.18
$\Delta M_{p,predict}$ ($\mu\text{g m}^{-3}$)	0.003	0.004	0.564	0.003	< 0.001	0.006	0.005
Total	$\Delta M_{p,predict} = 0.58 \mu\text{g m}^{-3}$			$\Delta M_{p,measured} = 1.25 \mu\text{g m}^{-3}$			
Average and Standard Deviation of four GUV222 on cycles							
$\Delta M_{p,predict} = 0.95 \pm 0.45 \mu\text{g m}^{-3}$				$\Delta M_{p,measured} = 1.84 \pm 0.67 \mu\text{g m}^{-3}$			

^a Y_{SOA} for linalool, β -pinene, α -terpinene, and terpinolene from Lee, et al. (2006). Y_{SOA} for α -pinene and limonene from Saathoff, et al. (2009). Y_{SOA} for ocimene was calculated as the average of values reported in Griffin, et al. (1999).

Fig. S17 shows the M_p production predicted from O_3 oxidation of the monoterpenes present in the restroom when GUV222 is on compared to what we measured. For four of the GUV222 on cycles we predict $1.0 \mu\text{g m}^{-3} \pm 0.5 \mu\text{g m}^{-3}$ organic aerosol would be formed compared to our measurements of $1.8 \mu\text{g m}^{-3} \pm 0.7 \mu\text{g m}^{-3}$. We excluded one of the cycles from this analysis because of the strong influence of NO on O_3 chemistry. For most of the cycles measured M_p was approximately 50 % greater than predicted M_p . We note that this calculation of predicted M_p from reacted terpenoid precursors and SOA yields assumes that the SOA yields of terpenoids + O_3 in the literature represent the yields we would expect to see in the restroom. Hydroxyl radicals and/or nitrate radicals produced from O_3 reactions could affect SOA yields in the restroom, and thus this calculation is an approximation of expected M_p production from GUV222. We show the comparison between of $\Delta M_{p,\text{predicted}}$ without wall loss included. Not including loss of $\text{VOC}_{\text{cond,g}}$ to walls (i.e., $f_{\text{cond}} + f_{\text{ACR}} = 1$) would over-predict $\Delta M_{p,\text{measured}}$ by a factor of three.

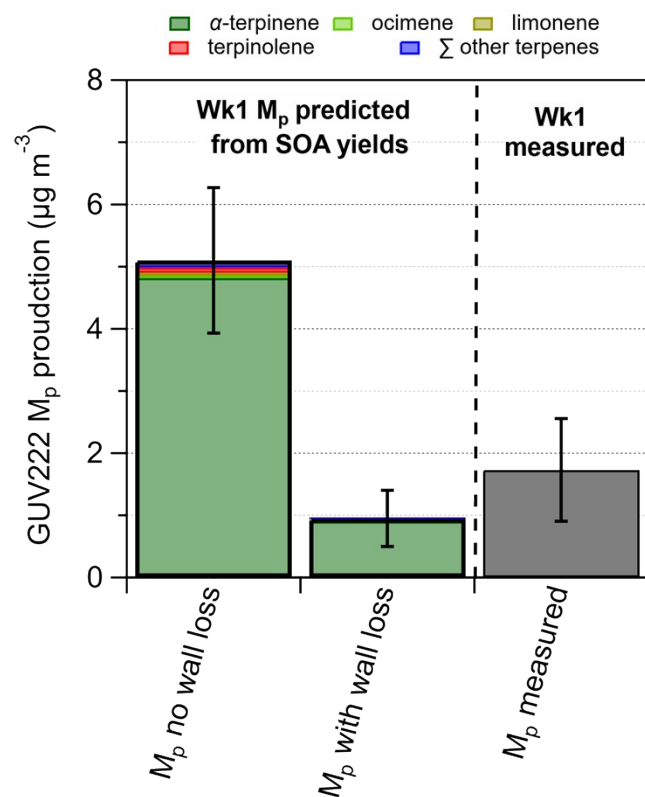


Fig. S17. M_p production predicted from SOA yield calculations compared to what was measured in Wk1. First two bars are predicted from reacted VOC concentrations and published organic aerosol yields. The third bar is what was measured.

References

1. K. Sekimoto *et al.*, Calculation of the sensitivity of proton-transfer-reaction mass spectrometry (PTR-MS) for organic trace gases using molecular properties. *International Journal of Mass Spectrometry* **421**, 71-94 (2017).
2. R. Holzinger *et al.*, Validity and limitations of simple reaction kinetics to calculate concentrations of organic compounds from ion counts in PTR-MS. *Atmospheric Measurement Techniques* **12**, 6193-6208 (2019).
3. A. R. Jensen, A. R. Koss, R. B. Hales, J. A. de Gouw, Measurements of VOCs in ambient air by Vocus PTR-TOF-MS: calibrations, instrument background corrections, and introducing a PTR Data Toolkit. *EGUosphere* **2023**, 1-38 (2023).
4. A. Lee *et al.*, Gas-phase products and secondary aerosol yields from the ozonolysis of ten different terpenes. *Journal of Geophysical Research: Atmospheres* **111**, (2006).
5. M. F. Link, R. Robertson, M. S. Claflin, D. Poppendieck, Quantification of Byproduct Formation from Portable Air Cleaners Using a Proposed Standard Test Method. *Environmental Science & Technology* **58**, 7916-7923 (2024).
6. H. Schwartz-Narbonne, B. Du, J. A. Siegel, Volatile organic compound and particulate matter emissions from an ultrasonic essential oil diffuser. *Indoor Air* **31**, 1982-1992 (2021).
7. H. Destailats *et al.*, Indoor secondary pollutants from household product emissions in the presence of ozone: a bench-scale chamber study. *Environmental Science & Technology* **40**, 4421-4428 (2006).
8. V. P. Barber *et al.*, Indoor air quality implications of germicidal 222 nm light. *Environmental Science & Technology* **57**, 15990-15998 (2023).
9. F. Bernard, V. Daële, A. Mellouki, H. Sidebottom, Studies of the gas phase reactions of linalool, 6-methyl-5-hepten-2-ol and 3-methyl-1-penten-3-ol with O₃ and OH radicals. *The Journal of Physical Chemistry A* **116**, 6113-6126 (2012).
10. D. Kim, P. S. Stevens, R. A. Hites, Rate constants for the gas-phase reactions of OH and O₃ with β -ocimene, β -myrcene, and α - and β -farnesene as a function of temperature. *The Journal of Physical Chemistry A* **115**, 500-506 (2011).
11. M. F. Link, A. Shore, B. H. Hamadani, D. Poppendieck, Ozone Generation from a Germicidal Ultraviolet Lamp with Peak Emission at 222 nm. *Environmental Science & Technology Letters* **10**, 675-679 (2023).
12. J. Burkholder *et al.*, "Chemical Kinetics and Photochemical Data for Use in Atmospheric Studies, Evaluation No. 19," (Jet Propulsion Laboratory, Pasadena, 2019).
13. D. Touhami *et al.*, Atmospheric degradation of ecologically important biogenic volatiles: investigating the ozonolysis of (E)- β -ocimene, isomers of α and β -farnesene, α -terpinene and 6-methyl-5-hepten-2-one, and their gas-phase products. *Journal of Chemical Ecology*, 1-14 (2024).
14. P. H. McMurry, D. Grosjean, Gas and aerosol wall losses in Teflon film smog chambers. *Environmental science & technology* **19**, 1176-1182 (1985).
15. W. H. Brune, The Chamber Wall Index for Gas-Wall Interactions in Atmospheric Environmental Enclosures. *Environmental science & technology* **53**, 3645-3652 (2019).

16. B. B. Palm *et al.*, In situ secondary organic aerosol formation from ambient pine forest air using an oxidation flow reactor. *Atmospheric Chemistry and Physics* **16**, 2943-2970 (2016).
17. S. M. Charan, Y. Huang, J. H. Seinfeld, Computational simulation of secondary organic aerosol formation in laboratory chambers. *Chemical reviews* **119**, 11912-11944 (2019).
18. J. E. Krechmer, D. Pagonis, P. J. Ziemann, J. L. Jimenez, Quantification of gas-wall partitioning in Teflon environmental chambers using rapid bursts of low-volatility oxidized species generated in situ. *Environmental Science & Technology* **50**, 5757-5765 (2016).
19. Y. Huang *et al.*, Unified theory of vapor–wall mass transport in Teflon-walled environmental chambers. *Environmental science & technology* **52**, 2134-2142 (2018).
20. X. Zhang *et al.*, Influence of vapor wall loss in laboratory chambers on yields of secondary organic aerosol. *Proceedings of the National Academy of Sciences* **111**, 5802-5807 (2014).
21. N. Fuchs, A. Sutugin, in *Topics in current aerosol research*. (Elsevier, 1971), pp. 1.
22. H. Saathoff *et al.*, Temperature dependence of yields of secondary organic aerosols from the ozonolysis of α -pinene and limonene. *Atmospheric Chemistry and Physics* **9**, 1551-1577 (2009).
23. R. J. Griffin, D. R. Cocker III, R. C. Flagan, J. H. Seinfeld, Organic aerosol formation from the oxidation of biogenic hydrocarbons. *Journal of Geophysical Research: Atmospheres* **104**, 3555-3567 (1999).